JCI insight

ARID1A-deficient bladder cancer is dependent on PI3K signaling and sensitive to EZH2 and PI3K inhibitors

Hasibur Rehman, … , Sooryanarayana Varambally, James E. Ferguson 3rd

JCI Insight. 2022. https://doi.org/10.1172/jci.insight.155899.

Research In-Press Preview Oncology

Graphical abstract

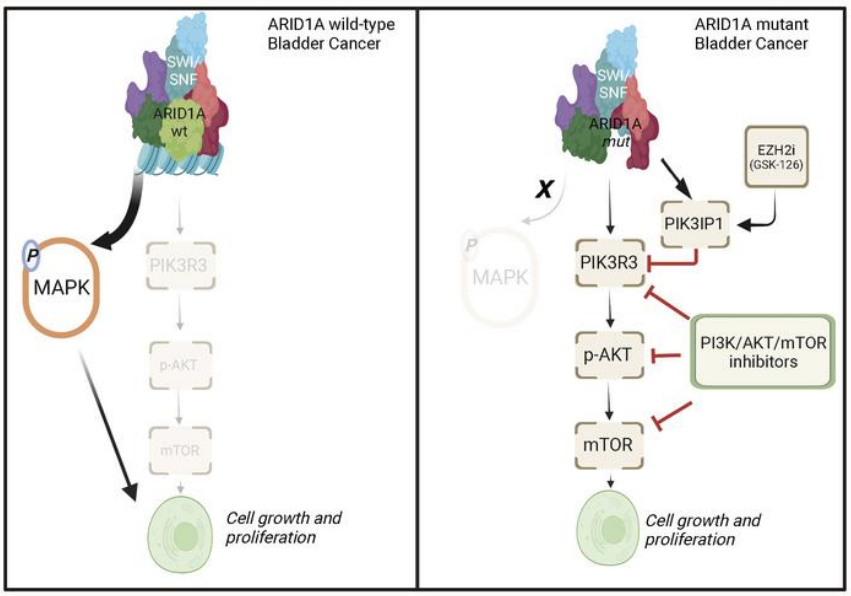

Find the latest version:

https://jci.me/155899/pdf

ARID1A-deficient bladder cancer is dependent on PI3K signaling and sensitive to EZH2 and PI3K inhibitors

Hasibur Rehman[1,2*], Darshan S. Chandrashekar[2,3,4*], Chakravarthi Balabhadrapatruni[3], Saroj Nepal[3], Sai Akshaya Hodigere Balasubramanya[3], Abigail K. Shelton[3], Kasey R. Skinner[3,5], Ai-Hong Ma[7], Ting Rao[7], Marie-Lisa Eich[8], Alyncia D. Robinson[3], Gurudatta Naik[2], Upender Manne[2,3], George J Netto[3], C. Ryan Miller[2,3], Chong-xian Pan[10], Guru Sonpavde[10], Sooryanarayana Varambally[2,3,4,#], James E. Ferguson III[1,2,11, #]

[1]Department of Urology, University of Alabama at Birmingham, Birmingham, AL, USA
[2]O'Neal Comprehensive Cancer Center, University of Alabama at Birmingham, Birmingham, AL, USA
[3]Department of Pathology, University of Alabama at Birmingham, Birmingham, AL, USA
[4]Informatics Institute, University of Alabama at Birmingham, Birmingham, AL, USA
[5]Neuroscience Curriculum, University of North Carolina at Chapel Hill, Chapel Hill, NC, USA
[6]Department of Biochemistry and Molecular Medicine, School of Medicine, UC Davis, Sacramento, CA 95817
[7]Department of Urology, Renmin Hospital of Wuhan University, Wuhan, China
[8]Institute of Pathology, University Hospital Cologne, Cologne, Germany.
[9]Department of Medicine, Lank Center for Genitourinary Oncology, Dana-Farber Cancer Institute, Harvard Medical School Boston, MA, USA
[10]Department of Medicine, Dana-Farber Cancer Institute, Harvard Medical School Boston, MA, USA
[11]Birmingham Veterans Affairs Medical Center, Birmingham, AL, USA.

[*]Shared Primary Authors

[#]Shared Senior Authors

Correspondence to:
James Ferguson, III M.D., Ph.D.
Department of Urology
O'Neal Comprehensive Cancer Center
Room # 410D
University of Alabama at Birmingham,
Birmingham, AL 35233, USA
jferguson@uabmc.edu
205-996-4186

Brief summary (25 words)
ARID1A-mutant bladder cancer is dependent on PI3K signaling and is sensitive to EZH2 and/or PI3K inhibition. Clinical trials in molecularly selected patients should be considered.

Abstract

Metastatic urothelial carcinoma is generally incurable with current systemic therapies. Chromatin modifiers are frequently mutated in bladder cancer, with *ARID1A*-inactivating mutations present in about 20% of tumors. EZH2, a histone methyltransferase, acts as an oncogene that functionally opposes ARID1A. In addition, PI3K signaling is activated in more than 20% of bladder cancers. Using a combination of in vitro and in vivo data, including patient derived xenografts, we show that ARID1A-mutant tumors are more sensitive to EZH2 inhibition than ARID1A-wild type tumors. Mechanistic studies reveal that: 1) ARID1A deficiency results in a dependency on PI3K/AKT/mTOR signaling via novel upregulation of a non-canonical PI3K regulatory subunit, PIK3R3, and downregulation of MAPK signaling, and: 2) EZH2 inhibitor sensitivity is due to upregulation of PIK3IP1, a protein inhibitor of PI3K signaling. We show for the first time that PIK3IP1 inhibits PI3K signaling by inducing proteasomal degradation of PIK3R3. Further, ARID1A deficient bladder cancer is sensitive to combination therapies with EZH2 and PI3K inhibitors, in a synergistic manner. Thus, our studies suggest that bladder cancers with *ARID1A* mutations can be treated with inhibitors of EZH2 and/or PI3K, and reveal mechanistic insights into the role of non-canonical PI3K constituents in bladder cancer biology.

Introduction

Bladder cancer is the 6th most common cancer in the US, and leads to ~18,000 deaths annually (1). Bladder cancer outcomes have been relatively stagnant despite the recent introduction of a number of new therapies including immune checkpoint blockade, antibody drug conjugates, and a targeted agent. Next generation sequencing has revolutionized our understanding of bladder cancer and provides an opportunity to develop personalized therapy (2,3). Nevertheless, so far only one targeted agent, erdafitinib, has been approved by the US Food and Drug Administration (FDA). Erdafitinib targets the fibroblast growth factor receptor 2/3 activating mutations or fusions which occur in less than 20% of advanced bladder cancer (4).

Sequencing datasets have revealed that genes encoding epigenetic/chromatin modifiers are frequently mutated in bladder cancer, as up to 90% of tumors have inactivating mutations in at least one chromatin-modifying enzyme (5). About 20% of bladder cancers have truncating and inactivating mutations in the AT Rich Interactive Domain 1A (*ARID1A*) gene, a member of the SWI/SNF chromatin modifying complex, making it one of the most frequently mutated epigenetic genes in bladder cancer. ARID1A is the DNA-binding component of the large multicomponent, 1.15 MDa SWI/SNF complex, which is important for ATP-dependent chromatin remodeling that generally results in increased transcriptional accessibility and modulates diverse gene programs and cellular processes including DNA repair, telomere cohesion, and immune recognition (reviewed in (6,7)). In human cancers, *ARID1A* shows predominantly nonsense truncating point mutations, resulting in lower protein levels and overall inactivation (6,8). Since ARID1A is the central DNA-binding component of SWI/SNF, it is thought that these heterozygous truncating mutations deactivate the complex either through incomplete complex assembly or a dominant

negative effect. Consistent with a gene dose-effect from heterozygous mutations, mice with heterozygous deletion of *ARID1A* are embryonic lethal (9).

We and others have shown that the histone methyltransferase Enhancer of Zeste Homolog 2 (EZH2) is over-expressed in many aggressive cancers, for which it is thought to drive growth and is thus considered an oncogene (10-13). EZH2 functions as the catalytic subunit of the polycomb repressive complex 2 (PRC2), which trimethylates lysine 27 on histone 3 (H3K27me3), resulting in transcriptional silencing of numerous genes including tumor suppressors (14-16). In aggressive bladder cancers, EZH2 expression is high and promotes proliferation of bladder cancer cells (17,18). In 2020, the EZH2 inhibitor tazemetostat received FDA approval for treatment of soft-tissue sarcomas, and lymphomas (19-21).

It has been shown in various models that mutations in *ARID1A* sensitize cells to EZH2 pharmacologic inhibition with the small molecule GSK-126 (22-24). We hypothesized that bladder cancer cells with *ARID1A* mutations would show sensitivity to EZH2 inhibition which could be utilized as a therapeutic target for patients with ARID1A-deficient bladder cancer.

Several studies suggest the cross-talk between ARID1A and PI3K pathways in clear cell ovarian cancer, and have shown that synthetic lethality by targeting EZH2 in *ARID1A*-mutated tumors correlates with inhibition of PI3K/AKT signaling (22,25). Of the four classes of PI3K, class I PI3K is the main subtype that phosphorylates phospho-inositide 4,5-bisphosphate to phospho-inositide 3,4,5-triphosphate (PIP3) in various cellular membranes, activates the downstream AKT/mTOR pathway, and plays important roles in cell survival, growth, proliferation, autophagy, differentiation, and metabolism (26-30). It is the downstream signal transducer of many cell surface receptors and abnormal activation of this pathway is often associated with oncogenesis. In bladder cancer, somatic alterations that lead to the activation of the PI3K/AKT/mTOR pathway

occur in over one third of cases (31). We have previously shown that activating alterations along the PI3K pathway are potential drivers and can possibly be targeted for the treatment of bladder cancer (32,33).

Class I PI3K enzymes are heterodimers consisting of a catalytic subunit and a regulatory subunit (reviewed in (34-36)). Binding of regulatory subunits to catalytic subunits stabilizes catalytic subunit proteins and allows for precise modulation of their enzymatic activity. There are two widely expressed catalytic subunit proteins coded for by two genes: *PIK3CA*/p110α and *PIK3CB*/p110β, and five regulatory subunit proteins expressed from three genes: *PIK3R1*/p85α/p55α/p50α, *PIK3R2*/p85β, and *PIK3R3*/p55γ. Of note, *PIK3R1* produces three separate proteins, with identical C-termini, through alternative splicing. Although the functional ramifications of the various heterodimer configurations and protein products of the regulatory subunits *PIK3R1* and *PIK3R2* have been fairly well characterized (27,29), comparatively little is understood about the relative contributions of *PIK3R3*/p55γ or how it interacts preferentially with the catalytic subunits p110α or p110β, or potentially competes with other regulatory subunits (28). Furthermore, PI3K inhibitors with relative specificity for p110α have been developed to maximize the therapeutic ratio relative to pan-class I inhibitors. But whether they are effective against heterodimers containing *PIK3R3*/p55γ is not well understood. Our studies add significantly to the understanding of the role of PIK3R3 in PI3K biology.

Overall, our investigations reveal a molecular dependence of ARID1A-deficient bladder cancers on PI3K/AKT signaling due to upregulation of *PIK3R3* and show a synergistic anti-tumor activity of EZH2 and PI3K inhibitors, suggesting that this combination could be re-purposed for the treatment of bladder cancer with alterations along these pathways which occur in over 40% of bladder cancer patients.

Results

ARID1A inactivating mutations in bladder cancers

To assess the prevalence of *ARID1A* mutations in bladder cancer, we performed in silico mutation analysis via cBioPortal (http://www.cbioportal.org/), using the Memorial Sloan Kettering Cancer Center bladder cancer sequencing dataset and the TCGA dataset. This analysis indicated that up to 29% of bladder cancers have nonsense or truncating mutations in *ARID1A* (Supplemental Figure S1A). Furthermore, *ARID1A*-mutated (herein referred to as ARID1A*mut*) bladder cancers express high levels of EZH2, consistent with previous findings that EZH2 expression is upregulated in bladder cancer (Supplemental Figure S1B). Our analysis of the COSMIC cell line dataset (Wellcome Trust Sanger Institute, UK) suggested that various bladder cancer cell lines harbored mutations in *ARID1A*. Among these, HT1376 has a frameshift deletion, and VM-CUB1 has a nonsense substitution mutation. Other bladder cancer cells (T24, RT-112, and 5637) do not have mutations in the *ARID1A* gene. Further, cell lines harboring truncating mutations in *ARID1A* show lower levels of the ARID1A protein, without differences in EZH2 or EZH2 methyltransferase activity (Figure 1A).

ARID1A mutation is associated with sensitivity to EZH2 inhibitors in vitro and in vivo

GSK-126 is a specific, small molecule inhibitor of EZH2. To investigate its effect on proliferation of ARID1A*mut* bladder cancer cells, we performed viability and proliferation assays using cell lines with and without mutations in *ARID1A*. The IC50s for ARID1A*mut* bladder cancer cells HT1376 (2.5 μM) and VM-CUB1 (2.8 μM) were much lower than ARID1A*wt* cells T24 (8.3 μM), 5637 (7.6 μM), and RT112 (7.8 μM) (Figure 1B). There were similar differences using proliferation assays (Figure 1C and Supplemental Figure S2A-B) and colony formation assays

(Supplemental Figure S2C). To confirm that the concentrations used were effective in inhibiting the histone methyltransferase activity of EZH2, we performed immunoblot analysis for the EZH2 methyltransferase product, H3K27me3. As expected, GSK-126 lowered H3K27me3 levels in all bladder cancer cell lines (Supplemental Figure S2A). Thus, at these concentrations, GSK-126 could efficiently inhibit EZH2-dependent histone methylation, but only ARID1A*mut* bladder cancer cells were sensitive while ARID1A*wt* cells were resistant.

To determine the anti-tumor activity in vivo, we performed murine xenograft experiments with human ARID1A*mut* and ARID1A*wt* bladder cancer cells. Consistent with the in vitro findings, systemic GSK-126 treatment effectively inhibited histone methylation in both ARID1A*wt* and ARID1A*mut* tumors (Supplemental Figure S3A**)**, but it only suppressed growth of ARID1A*mut* tumors but not ARID1A*wt* tumors (Figure 1D). We previously reported that patient-derived xenografts (PDXs) retained the morphology and genomic fidelities and are considered one of the best models in reflecting patient cancers' pharmacologic susceptibilities (32). To evaluate the translational significance of this association, we tested the GSK-126 sensitivity of PDXs harboring ARID1A*wt* and mutant alleles. ARID1A*mut* PDX models were sensitive to GSK-126, but ARID1A*wt* models were resistant (Figure 1E).

ARID1A knockdown induces GSK-126 sensitivity in ARID1A*wt* bladder cancer cells

To mimic the functional ramifications of inactivating mutations in a more genetically defined model, we generated shRNA-mediated stable knockdown of ARID1A in all 3 ARID1A*wt* cell lines (herein referred to as ARID1A*kd* cells) (Figure 2A). Although ARID1A knockdown did not affect cell viability/proliferation at baseline, it did result in higher sensitivity to GSK-126, as evidenced by lower viability (Figure 2B), decreased proliferation (Figure 2C), and decreased

colony formation (Supplemental Figure S4A). Further, after treatment with GSK-126, apoptosis and autophagy were activated in ARID1A*kd* cells, but not in ARID1A*wt* cells, as evidenced by increased cleaved caspase 3 and LC3BII immunoblotting (Figure 2D). These ARID1A*kd* cells were then used to generate xenografts to test their sensitivity to EZH2 inhibition in vivo. Although RT112 and 5637 ARID1A*wt* xenografts are resistant to GSK-126 (Figure 1D), ARID1A*kd* cells were sensitive, and their growth was nearly completely inhibited (Figure 2E and Supplemental Figure S4B). To confirm that EZH2 inhibitor sensitivity was generalizable to other drugs, we performed these dose response cell viability experiments using three different EZH2 inhibitors: CPI-1205 and EPZ-6438, both SAM-specific inhibitors that inhibit EZH2 catalytic activity in a manner similar to GSK-126, and MAK683, an EED binding inhibitor which disrupts the PRC2 complex leading to EZH2 protein degradation. Similar results were found (Supplemental Figure S4C-D).

Next, we performed reconstitution experiments wherein ARID1A*mut* cells were stably transduced with ARID1A-expressing constructs via lentivirus (Figure 2F). Cell viability assays showed that ARID1A overexpression/reconstitution induced GSK-126 resistance (Figure 2G). Activity of GSK-126 was confirmed by immunoblot for H3K27Me3 (Figure 2F). Xenograft studies showed that ARID1A-reconstituted mutant cell lines were resistant to GSK-126 in vivo (Figure 2H and Supplemental Figure S4E). Thus, we confirmed that sensitivity of bladder cancer cells to EZH2 inhibition is dependent on ARID1A deficiency.

Investigating the mechanisms of EZH2 sensitivity in ARID1A-deficient bladder cancer cells

We hypothesized that ARID1A-deficient cells are more sensitive to GSK-126 due to transcriptional upregulation of specific tumor suppressors that remain transcriptionally repressed

in ARID1A*wt* cells. To test this hypothesis, we performed RNAseq whole-transcriptomic analysis comparing ARID1A*wt* and ARID1A*kd* RT112 bladder cancer cells with GSK-126 treatment or control. We isolated RNA after 24 h to capture the early/primary transcriptional effects of GSK-126 while avoiding secondary effects due to lower viability and apoptosis initiation at later time points. Although there was a large number (>1000) of differentially expressed genes when comparing untreated ARID1A*wt* to ARID1A*kd* cells at baseline (as expected given the function of ARID1A as a master transcriptional regulator), there were comparatively fewer (<70) differentially expressed genes in response to GSK-126 treatment. We specifically evaluated differentially expressed genes in GSK-126-treated ARID1A*kd* cells that were not differentially expressed following treatment of ARID1A*wt* cells (Figure 3A). Of these genes, one tumor suppressor, *PIK3IP1*, was particularly notable, as it attenuates PI3K/AKT/mTOR signaling through a direct inhibition of *PIK3CA*/p110α (37). This raised the hypothesis that ARID1A-deficient cells are dependent on PI3K signaling for survival, perhaps through an upregulation of PI3K constituents. To this end, we investigated the transcriptional levels of all of the class I PI3K subunits using the RNAseq data and found that ARID1A*kd* leads to upregulation of *PIK3R3*, a relatively uncharacterized regulatory subunit of PI3K that forms heterodimers with PIK3CA and modulates its activity (Figure 3B). We confirmed the RNAseq data via qRT-PCR and immunoblots and showed that ARID1A*kd* results in activation of the PI3K/AKT/mTOR pathway (as evidenced by higher levels of pAKT (Thr 308), phospho-mTOR, p4EBP1, and pS6K), and that GSK-126 treatment in ARID1A*kd* cells prevents this activation, which correlates with PIK3IP1 upregulation (Figure 3C). Furthermore, PIK3IP1 upregulation correlates with downregulation of *PIK3R3*/p55γ and *PIK3R1*/p85/p50α (Figure 3C) without a significant change in mRNA levels (Supplemental Figure S5A-B), suggesting a post-translational mechanism. Protein levels of other class I PIK3

subunits (p110α, p110β, and p85β) were relatively unchanged (Figure 3C). To determine if ARID1A is present at the promoters of *PIK3R3* and *PIK3IP1*, we performed Cleavage Under Targets and Release using Nuclease (CUT&RUN) using two independent ARID1A antibodies and confirmed that ARID1A is present at the promoters of both *PIK3R3* and *PIK3IP1* (Supplemental Figure S5C-D)

We hypothesized that ARID1A*kd* cells downregulate other pro-proliferation pathways to become dependent on PI3K/AKT/mTOR signaling for survival. This hypothesis was based on the following findings: 1) PI3K/AKT/mTOR signaling is increased in ARID1A*kd* cells (Figure 3C), but proliferation of ARID1A*kd* cells is no different from wild-type cells (Figure 2C). 2) GSK-126 treatment resulted in decreased viability of ARID1A*kd* cells (Figure 2C) despite decreasing pAKT levels only to levels found in ARID1A*wt* cells (which are resistant to GSK-126) (Figure 3C). We thus empirically compared the relative activation of pro-proliferation pathways prominent in bladder cancer biology and found that pERK, pJNK, and phospho-p38 were all lower in ARID1A*kd* cells (Figure 3D).

To test whether the intact SWI-SNF complex (aka BAF) was necessary to prevent GSK-126 sensitivity, we knocked down key SWI-SNF components (BRG, BAF47, BRM) via siRNA in RT112 cells. Knockdown of each component was associated with upregulation of PIK3R3 at baseline, and upregulation of PIK3IP1 after treatment with GSK-126 (Figure 3E).

Next, we tested whether ARID1A reconstitution/overexpression in ARID1A*mut* cells prevented this process. In ARID1A*mut* cells, pAKT and PIK3R3 levels were high at baseline and treatment with GSK-126 decreased these levels (which correlated with PIK3IP1 upregulation) (Figure 4A). As hypothesized, ARID1A reconstitution lowered PIK3R3 and pAKT levels at baseline, and

prevented PIK3IP1 upregulation upon GSK-126 treatment (Figure 4A). Furthermore, when comparing ARID1A*mut* and wild-type cells, ARID1A*mut* lines showed higher levels of pAKT, PIK3R3, PIK3R1/p85α/p50α, and p85β, and lower MAPK activation, indicative of an intrinsic shift in pro-growth signaling dependent on ARID1A status (Figure 4B). Next, we sought to determine if ARID1A deficiency correlated with PIK3R3 upregulation and PI3K/AKT pathway activation in human bladder cancers. Using lysates of three matched pairs of human bladder cancers and adjacent normal tissue, as well as six unmatched samples, we determined that tumors deficient in ARID1A protein had elevated PIK3R3 and pAKT levels (Figure 4C). Furthermore, using lysates from PDX models harboring ARID1A*wt* or -*mut* alleles, we determined that ARID1A mutant/deficient tumors had elevated PIK3R3 and pAKT levels, and decreased pERK levels (Figure 4D). These findings suggest that in bladder cancer cells, ARID1A deficiency induces a biologic dependency on PI3K/AKT signaling that can be pharmacologically targeted through EZH2 inhibition and upregulation of PIK3IP1.

PIK3IP1 upregulation is necessary and sufficient for GSK-126-mediated cell death in ARID1A-deficient bladder cancer cells

To determine if PIK3IP1 upregulation is necessary and sufficient for GSK-126 sensitivity in ARID1A-deficient bladder cancer cells, we generated an array of dual ARID1A/PIK3IP1 stable knockdown cells, and ARID1A*kd*/PIK3IP1 stable overexpression cells (Figure 5A, 5C). Stable knockdown of PIK3IP1 in ARID1A*kd* cells prevented GSK-126-mediated downregulation of PIK3R3 and pAKT and rescued/reversed the sensitivity to GSK-126, compared with empty vector (Figure 5B). We hypothesized that stable overexpression of PIK3IP1 in ARID1A*kd* cells would result in cell death, so we generated overexpression systems using a two-vector doxycycline-inducible system. Overexpression of PIK3IP1 in ARID1A*kd* cells was sufficient to downregulate

PIK3R3 and pAKT levels (Figure 5C), and it completely blocked cell growth (Figure 5D). As the downregulation of PIK3R3 upon PIK3IP1 overexpression was not associated with any changes in transcript levels (Figure 3, and Supplemental Figure S5A), we hypothesized that this was due to ubiquitin-mediated proteasome degradation. To test this, we treated ARID1A*kd*/PIK3IP1-inducible RT112 cells with doxycycline and the proteasome inhibitor MG-132 and found that proteasomal inhibition prevented PIK3IP1-dependent downregulation of PIK3R3 protein (Figure 5E). Finally, using ARID1A*kd*/PIK3IP1-inducible RT112 cells that had been treated with doxycycline and MG-132, we found that PIK3R3 immunoprecipitates contained PIK3IP1 and poly-ubiquitin moieties (Figure 5F). Together, these data suggest that PIK3IP1 binds to PIK3R3 and promotes poly-ubiquitination and degradation of PIK3R3.

ARID1A-deficiency correlates with sensitivity to PI3K inhibitors, which are synergistic with EZH2 inhibitors.

To assess whether ARID1A deficiency sensitizes bladder cancer cells to PI3K inhibitors, we performed dose-response cell viability experiments comparing ARID1A*wt* and ARID1A*kd* cell lines in the presence of alpelisib (a PI3K alpha-selective inhibitor), pictilisib (a PI3K pan-class I inhibitor), or dactolisib (a dual PI3K/mTOR inhibitor). For all inhibitors tested, ARID1A*kd* cells were more sensitive than ARID1A*wt* cells (Figure 6A, and Supplemental Figure S6A-C). Since combination therapies are often utilized to maximize therapeutic benefit at lower doses and to avoid off-target side effects at higher doses, we tested the synergy of GSK-126 and pictilisib using a dose-response cell viability assay with three different ARID1A*kd* cell lines and found that each demonstrated synergy (based on Combination Indices (C.I.) <0.85 calculated by the Chou-Talalay method) (Figure 6B and Supplemental Fig S6D). ARID1A*mut* cells were more sensitive to pictilisib than ARID1A*wt* cells (Figure 6C). These data suggest that ARID1A-deficient bladder

cancers can be therapeutically targeted with EZH2 or PI3K inhibitors alone, or ideally in combination.

PIK3R3 upregulation is necessary and sufficient for PI3K/AKT pathway activation and increased bladder cancer cell proliferation.

To determine if PIK3R3 upregulation is necessary and sufficient for PI3K/AKT pathway activation and rapid cell proliferation, we generated dual ARID1A/PIK3R3 stable knockdown cells, and ARID1A*wt* cells stably overexpressing PIK3R3 along with empty vector controls (Figure 7). Knockdown of PIK3R3 decreases pAKT and pS6k levels in ARID1A*kd* cells (Figure 7A) and inhibits growth of ARID1A*kd* but not ARID1A*wt* cells (Figure 7B). Stable overexpression of PIK3R3 in ARID1A*wt* cells is sufficient to increase pAKT levels (Figure 7C) and results in increased proliferation; however, these cells are not more sensitive to GSK-126 (Figure 7D and Supplemental Figure S7A). Immunoblot analysis confirmed the activity of GSK-126 in these cells as evidenced by lower H3K27me3 levels (Figure 7E). Furthermore, PIK3R3 overexpression resulted in resistance to PI3K inhibitors **(**Figure 7F and Supplemental Figure S7B), and xenografts with PIK3R3 overexpression grew faster than xenografts transfected with empty vector (Figure 7G, and Supplemental Figure S7C). Finally, utilizing the TCGA dataset, we found that ARID1A*mut* tumors have higher transcript levels of PIK3R3 than ARID1A*wt* tumors (Supplemental Figure S7D).

Together, these data suggest that PIK3R3 upregulation in ARID1A*kd* cells drives activation of the PIK3/AKT/mTOR pathway, a process sufficient to increase proliferation in ARID1A*wt* cells. However, due to the lack of dependency of ARID1A*wt* cells on the PI3K/AKT pathway (as

evidenced by intact ERK, JNK, and p38 signaling cascades), PIK3R3 upregulation alone does not result in pharmacologic vulnerabilities in the PI3K/AKT pathway (see graphical abstract).

Discussion

Metastatic urothelial carcinoma is generally incurable, with modest survival benefit provided by cisplatin-based first-line chemotherapy (median survival ~15 months) (38). Durable benefits with post-platinum PD-1/L1 inhibitors extend survival to a minority of patients (~20%), and the median survival is <1 year (39). Third-line salvage therapies (e.g. Enfortumab Vedotin, Sacituzumab Govitecan) are not curative but provide incremental benefits with median overall survival of ~1 year. However, the first targeted agent for bladder cancer, erdafitinib, is active and is approved to treat post-platinum patients with activating somatic *FGFR2/3* mutations or fusions, which are seen in ~15% of patients (40). Hence, new therapeutic approaches are needed for treatment of bladder cancer patients. These will be achieved with better understanding of therapeutically actionable targets and mechanisms of resistance. Given the heterogeneity of this malignancy with multiple genomic alterations, there remains a role for rational approaches targeting these subsets of patients.

ARID1A is frequently mutated across a wide variety of human cancers, including bladder, gastric, pancreatic, and ovarian cancers (6,7). As ARID1A is the DNA-binding subunit of the large ~1.15MDa SWI/SNF multi-subunit complex, its loss through nonsense mutations is thought to result in complex disassembly. Mutation of just one allele of *ARID1A* results in embryonic lethality for mice and contributes to tumorigenesis (8,9). Thus, tightly controlled protein levels of ARID1A are critical for normal development and disease prevention.

Although loss of tumor suppressors such as ARID1A are difficult to target directly, oftentimes these losses result in therapeutic vulnerabilities that can be targeted through a synthetic lethality approach. For various bladder cancer cell lines with ARID1A-truncating mutations or shRNA-mediated depletion, our experiments revealed that EZH2 inhibition is synthetically lethal for

bladder cancer cells with ARID1A deficiency. There are similar findings for OCCCs (22). Other groups have investigated this relationship in bladder cancer cells and come to somewhat different conclusions (41). The cells in these studies, however, were treated with EZH2 inhibitor for only 2-3 days and showed no specific sensitivity for EZH2 inhibition, whereas we found that at least 6-8 days of treatment is necessary to see substantial differences in viability. This could explain the differences between these results.

Pharmacologic inhibitors of EZH2 are currently being investigated in a variety of tumor types, including lymphomas, sarcomas, and advanced treatment-resistant solid tumors (reviewed in (20)). B-cell lymphomas often have activating mutations in EZH2, and some sub-types of sarcomas have mutations in SWI-SNF subunits *SMARCB1* (BAF47) or *SMARCA4* (BRG1). In fact, the EZH2 inhibitor tazemetostat was approved by the FDA in 2020 for the treatment of advanced epithelioid sarcoma (42). Thus, there is a rationale to re-purpose EZH2 inhibitors for the pharmacologic treatment of patients with bladder cancers harboring somatic truncating mutations in *ARID1A*. A phase I/II trial is currently investigating the combination of tazemetostat/pembrolizumab in patients with molecularly unselected, advanced urothelial carcinoma (clinicaltrials.gov NCT03854474) and another trial is investigating tazemetostat alone in advanced solid tumors harboring an ARID1A mutation (NCT05023655). The results herein suggest that sub-group analyses of these and other EZH2 inhibitor trials should focus on bladder cancer patients with ARID1A-deficient tumors.

We discovered that ARID1A mutations and/or deficiency leads to a dependency on PI3K/AKT/mTOR signaling via upregulation of PIK3R3 and downregulation of MAPK signaling. The PI3K/AKT/mTOR pathway is involved in bladder tumorigenesis, as a substantial proportion of these tumors have activating mutations in PIK3CA (2). Among the regulatory subunits, PIK3R3

is least characterized. Little is understood about how it preferentially interacts with the various catalytic subunits, how it competes with other regulatory subunits, and how heterodimers containing PIK3R3 function in the presence of PI3K pharmacologic inhibitors. To determine if PIK3R3 upregulation in ARID1A*def* cells is specific to bladder cancer, we performed an in silico meta-analysis focused on the differential expression of PI3KR3 in all publicly available transcriptomic datasets comparing ARID1A-deficient and wild-type cells. Using six separate data sets from six different cancer cell lines (including one OCCC), only one cell line (cholangiocarcinoma: HuCCT1) showed a statistically significant increase in PIK3R3 in ARID1A-deficient cells (Supplementary Figure S8) suggesting that the molecular mechanisms that lead to PIK3R3 upregulation in bladder cancer cells may be uncommon in other tumor types. Experiments are underway to determine these mechanisms. Downregulation of MAPK pathways in ARID1A-deficient endometrial carcinoma has been described (43), but whether this is universal amongst ARID1A-deficient tumors remains to be determined.

Inhibition of EZH2 in ARID1A*def* bladder cancer cells results in upregulation of PIK3IP1, an endogenous inhibitor of PI3K signaling. Although other data suggest that PIK3IP1 functions through direct binding and inhibition of PI3K catalytic subunit activity (37,44), we reveal a novel mechanism by which PIK3IP1 expression induces proteasomal degradation of the regulatory subunit PIK3R3. In OCCCs, ARID1A and EZH2 compete (along with histone deacetylase 2) to modulate expression of the *PIK3IP1* gene (22,25). However, while PIK3IP1 protein levels are increased in response to GSK-126 in ARID1A*def* cells in both OCCC and bladder cancer, the effects of ARID1A levels on PIK3IP1 expression are opposite between the cell types. Factors contributing to this difference and the ramifications of this difference are being investigated.

In conclusion, ARID1A-deficient bladder cancers are dependent on PI3K signaling, which can be pharmacologically targeted with EZH2 and/or PI3K inhibitors. Our results show a novel role for PIK3R3 as an oncogene in bladder cancer biology. Finally, these data demonstrate that the role of PIK3IP1 in the sensitivity of ARID1A*def* cells to EZH2 inhibitors may be shared amongst multiple tumor types. In sum, clinical applications targeting these molecules in ARID1A-deficient bladder cancers should be pursued.

Materials and Methods

Experimental Design

Cell lines and reagents

Bladder cancer cell lines HT1376 (RRID: CVCL_1292), T24 (CVCL_0554), and 5637 (CVCL_0126) were obtained from ATCC (Manassas, VA, USA), and RT112 (CVCL_1670) and VM-CUB1 (CVCL_1786) from DSMZ (Braunschweig, Germany). Cell lines were authenticated by the vendors and tested for mycoplasma prior to use. These were grown in Dulbecco's 90% MEM (4.5 g/L glucose) with penicillin–streptomycin (100 U/ml) and 10% fetal bovine serum (Sigma-Aldrich, St Louis, MO, USA) in 5% CO_2 incubators. GSK-126 (Catalog # HY-13470), alpelisib (HY-15244), and dactolisib (HY-50673) were obtained from Medchem Express (Monmouth Junction, NJ). Pictilisib (#S1065), MG132 (S2619), MAK-683, EPZ-6438, and CPI-1205 were obtained from Selleckchem (Houston, TX, USA). Captisol (RC-0C7-020) was obtained from CyDex Pharmaceuticals, (Lawrence, KS, USA).

Cell proliferation and dose response assays

After exposure to drugs as indicated, cell viability was measured by luminescence using CellTiter-Glo® 2.0 (Promega, Madison, WI, USA), according to manufacturer's instructions. Luminescence was measured on a Synergy HTX multi-mode reader (BioTek Instruments, Inc., Winooski, VT, USA). For dose-response experiments, media/drug was replenished every other day. Percent viability of cells was calculated as follows: % viability = 100 − (Treated relative luminescence unit/Non-treated RLU)/100). For drug combination studies, data were analyzed for synergistic interactions using CompuSyn software (ComboSyn, Inc.) and the Chou–Talalay method (45).

RNA isolation and RNAseq analysis

Total RNA from cultured cells was extracted with Direct-zol RNA miniprep kits (Zymo Research). Library preparation was performed with purified, extracted RNA using KAPA Stranded mRNA-seq kits (Kapa, Biosystems, Wilmington, MA) according to the manufacturer's protocol. Twelve samples with various adapters were pooled to create a 15-nM multiplexed sample for sequencing. This pooled sample was diluted to 1.65 pM and spiked with 1% PhiX bacterial genome as a positive control for alignment. High-throughput sequencing with 75-bp single-end reads was performed on an Illumina NextSeq 550 using an Illumina NextSeq 500/550 High Output Kit. Reads were aligned to the human transcriptome GENCODE v32 (GRCh38.p13) using STAR and counted using Salmon. Normalization and differential expression analysis were performed using the R package DESeq2. Genes for which there were fewer than three samples with normalized counts ≤ five were filtered out of the final data set. A Benjamini-Hochberg-adjusted p-value of < 0.05 and a log2 fold change of 1 were thresholds used to identify differentially expressed genes between treatment conditions. Conditions were run in biologic triplicates.

Xenograft tumor growth assays

For tumor xenograft experiments, *NU/J nu/nu* male and female mice aged 6-8 weeks (n = 5 for each group) from Jackson Laboratories (RRID:IMSR_JAX:002019) were injected subcutaneously into the right dorsal flanks with human bladder cancer cells (1-2 × 10^6 cells in 50 µL of incomplete media without FBS, and 50 µL of Matrigel, #354277 from Corning). Tumor growth was measured with Vernier calipers and recorded weekly. Tumor volume was calculated with the formula: 0.5 × tumor length × tumor width^2. Animals were randomized prior to treatment initiation. GSK-126 was administered intraperitoneally at a dose of 100 mg/kg daily after tumor volume reached 150 to 200mm^3. The final volume of drug/vehicle was 0.2 ml per 20g body weight in 20% Captisol, adjusted to pH 4-4.5 with 1 N acetic acid. Mouse body weights were monitored to assess toxicity.

At the end of the treatment tumors were excised, weighed, processed, and stored for downstream molecular analysis. Statistical analyses were conducted by two-tailed Student's t-tests.

Bladder cancer patient-derived xenografts

Bladder cancer patient-derived xenograft (PDX) models were provided by The Jackson Laboratory (JAX, Bar Harbor, ME). PDXs were developed through subcutaneous implantation of clinical tumor tissues into immunodeficient NOD.Cg-*Prkdcscid Il2rgtm1Wjl*/SzJ (NSG; RRID:IMSR_JAX:005557) female mice, followed by serial passaging as previously described (32). All experiments utilized PDX models within the first five passages.

PDX bladder cancer mouse models

Six- to 8-week-old female beige SCID mice bearing bladder cancer PDX (UC Davis ID# BL0293 or JAX Model # TM00016; UC Davis ID#BL0269, or JAX Model #TM00015) were utilized. Fresh PDX specimens (3–5mm^3) were implanted subcutaneously into the flanks of SCID mice. Experimental design followed the xenograft protocol as above.

For immunoblot analysis, various PDX tissues from tumors harboring *ARID1A* wild-type or mutant alleles were purchased from Jackson Laboratories. ARID1A*wt* PDX included: TM00015 (sample #1 in Figure 4D), TM00024 (2), TM00013 (3), TM00020 (4), J000107333 (5), TM01029 (6) and ARID1A*mut* PDX included: TM00016 (7), J000109799 (8), J000108112 (9), J000102326 (10) and J000100646 (11).

Immunoblot analyses

Antibodies, listed in Table 1 in Supplementary Methods, were used at dilutions optimized in our laboratory. For immunoblot analysis, protein samples were separated by sodium dodecyl sulfate-

polyacrylamide gel electrophoresis and transferred onto Immobilon-P PVDF membranes (EMD Millipore, Billerica, MA, USA). The membranes were incubated for 1 h in blocking buffer (Tris-buffered saline, 0.1% Tween (TBS-T), 5% nonfat dry milk), followed by incubation overnight at 4°C with the primary antibody. After a wash with TBS-T, the blots were incubated with a horseradish peroxidase-conjugated secondary antibody and signals were visualized by Luminata Crescendo chemiluminescence western blotting substrate as per the manufacturer's protocol (EMD Millipore).

Immunoprecipitation

Cell lysate (400µg) was incubated with either anti-PIK3R3 or IgG control (5µg) overnight at 4ºC with rotation. Then, 25µL of washed Protein A/G magnetic beads (ThermoFisher) were added and incubated 1-2h at 4° with rotation. The bead/immune complex was then washed three times with 20 mM Tris-HCl, 150 mM NaCl, 2 mM EDTA (pH 8.0). The immunoprecipitated proteins were eluted by boiling beads in the Laemmli buffer and analyzed by immunoblot analysis.

Preparation of human bladder cancer lysates

As previously described (46), after IRB approval at the University of Alabama-Birmingham (#X120917005), written informed consent from patients, and after pathologic stage and grade determination, protein lysates were prepared from human bladder cancer samples and surrounding normal mucosa, using tissues from radical cystectomies.

RNA Interference and Transfection

As described previously (47), small interfering RNA (siRNA) duplexes (listed in Supplemental Methods Table 2) were purchased from Dharmacon (Horizon Discovery), Lafayette, CO (GE

Healthcare). Transfections were performed with Lipofectamine RNAiMAX (Life Technologies) reagent per manufacturer's instructions. Seventy-two hours after the transfection, cells were harvested for immunoblot analysis.

ARID1A shRNA lentivirus production

High-titer lentivirus was generated following a protocol previously described in detail (48). In brief, pMD2.G (Addgene, MA, USA, #12259), psPAX2 (Addgene, #12260) and pLKO.1-shARID1A (MISSION shRNA (Sigma-Aldrich), (either TRCN0000059089 (sh1), or TRCN0000059090 (sh2)) were used. ARID1Ash2 was used in experiments where one shRNA was utilized. For negative control pLKO.1 GFP shRNA (Addgene #30323) was used. These lentiviruses were used to infect ARID1A wild-type bladder cancer cells which were then selected for stably transfected clones using puromycin (Gibco, ThermoFisher) at a concentration of 1-2μg/ml for 2 weeks. Stable clones were selected and tested for ARID1A knockdown efficiency via immunoblots.

Generation of ARID1A-expressing lentiviruses

ARID1A cDNA-expressing lentiviruses were constructed using the protocol described above. pLenti-puro-*ARID1A* (from Addgene #39478) or empty vector (p-Lenti-puro, Addgene #39481)-containing lentiviruses were used to infect *ARID1A* mutant bladder cancer cells which were then selected for stably transfected clones using puromycin (Gibco, ThermoFisher) at a concentration of 1-2μg/ml for 2 weeks. Stable clones were selected and tested for ARID1A overexpression via immunoblots.

Plasmids and antibodies

A human PIK3IP1 stable overexpression system was custom-designed and purchased from VectorBuilder (Chicago, IL, USA). This is a 2-vector system, with one vector expressing doxycycline-inducible transcriptional modulators (pLV[Exp]- CMV>tTS/rtTA/Hygro) and a second vector containing h*PIK3IP1* downstream from an inducible promoter (pLV[Exp]-Neo-TRE> *hPIK3IP1*[NM_052880.5]). *PIK3R3* overexpression vectors were custom-designed and purchased from Vector Builder (pRP[Exp]-Neo-CMV>*hPIK3R3*[NM_003629.4], along with an empty vector control (pRP[Exp]-Neo-CMV>ORF_Stuffer). PIK3R3 shRNA-containing lentivirus was purchased from Sigma-Aldrich (TRCN0000195671) (sh1) and TRCN0000033290 (sh2)), with pLKO.1-CMV-Neo vector as empty vector control. PIK3R3 sh1 was used in experiments where one shRNA is indicated. PIK3IP1 shRNA-containing lentivirus was purchased from Sigma-Aldrich (TRCN0000138560) with pLKO.1-CMV-Neo vector as empty vector control. The infected cells were selected with puromycin (1-2 μg/ml), neomycin (800-900 μg/ml) and hygromycin (150-200 μg/ml) as needed.

The antibodies used are listed in Supplemental Table 1 in Supplementary Methods. Of note, the PIK3R1 antibody was chosen given its epitope in the C-terminus and its capacity to detect all three splice variants of the gene, p85α/p55α/p50α. Using this antibody, we detected p85α and p50α, not p55α.

Statistical analyses

All results are representative of at least three biologic replicates, unless otherwise specified. All data points are the means +/- standard deviations representative of at least three technical replicates, unless otherwise specified. Two-way ANOVA or two-tailed Student's t-tests were performed using GraphPad Prism v7.03 to determine significant differences between control and

experimental groups, as mentioned in the figure legends. P-values of <0.05 were considered statistically significant.

Study Approval

Animal studies were performed at University of Alabama-Birmingham and University of California-Davis with approval of the Institutional Animal Care and Use Committee (protocol #19564 at UC-Davis and #21573 at UAB).

Data Availability

The RNAseq data generated in this study are publicly available in Gene Expression Omnibus (GEO) at GSE183777.

Author Contributions:

HR: Experimental design, data generation, experimental interpretation, manuscript preparation and review. Dr. Rehman was chosen as first listed co-author given his extensive data generation, and manuscript preparation.
DSC: Experimental design, data generation, experimental interpretation, manuscript preparation and review.
CB: Experimental design, data generation, experimental interpretation, manuscript preparation and review.
SN: Experimental design, data generation
SB: Experimental design, data generation
AS: Data generation, experimental interpretation, manuscript preparation and review.
KRS: Data generation, experimental interpretation, manuscript preparation and review.
AM: Data generation, experimental interpretation, manuscript preparation and review.
TR: Data generation, experimental interpretation, manuscript preparation and review
SA: experimental interpretation, manuscript preparation and review
MLE: Data generation, experimental interpretation, manuscript preparation and review.
ADR: Data generation, experimental interpretation, manuscript preparation and review.
GN: Data generation, experimental interpretation.
UM: Manuscript preparation and review.
GJN: Experimental interpretation, manuscript preparation and review. Project funding.
CRM: Experimental interpretation, manuscript preparation and review.
CXP: Experimental design, experimental interpretation, manuscript preparation and review, project funding.
GS: Experimental design, experimental interpretation, manuscript preparation and review, project funding.
SV: Experimental design, experimental interpretation, project funding, manuscript preparation and review.
JEF: Experimental design, experimental interpretation, project funding, manuscript preparation and review.

Acknowledgements:

Funding: The research reported in this article was supported in part by: Research Development Award from the U.S. Department of Veterans Affairs BLRD service (to JEF), Grant # 1I01 BX003840 (to CP), Department of Defense grant # W81XWH1910588 (to SV) and U54 Grant No: 1 U54 CA233306 (to CP). The contents do not represent the views of the U.S. Department of Veterans Affairs or the United States Government.

Graphical abstract was created with BioRender.com, with appropriate license release.

The authors would like to thank Don Hill for editing the manuscript.

List of Supplementary Materials

Supplementary Methods

Supplementary Figures

Supplementary Figure S1: Bladder cancer harbors high rates of ARID1A mutation, and high expression of EZH2.

Supplementary Figure S2: ARID1A mutation is associated with increased GSK-126 sensitivity.

Supplementary Figure S3: GSK-126 treatment effectively inhibits H3K27 trimethylation in xenograft tissues, and inhibits xenograft growth in ARID1Amut cell lines..

Supplementary Figure S4: ARID1A deficiency is necessary and sufficient for sensitivity to GSK-126.

Supplementary Figure S5: ARID1A presence and effects at PIK3R3 and PIK3IP1 loci.

Supplementary Figure S6: ARID1A deficiency sensitizes bladder cancer cells to PI3K inhibitors.

Supplementary Figure S7: PIK3R3 overexpression increases growth kinetics of ARID1Awt cells.

Supplementary Figure S8: PIK3R3 expression pattern in ARID1A mutated/altered cancer cell lines.

References

1. Siegel RL, et al. Cancer statistics, 2018. *CA Cancer J Clin.* 2018;68(1):7-30.
2. Robertson AG, et al. Comprehensive Molecular Characterization of Muscle-Invasive Bladder Cancer. *Cell.* 2017;171(3):540-556 e525.
3. Hurst CD, Knowles MA. Mutational landscape of non-muscle-invasive bladder cancer. *Urol Oncol.* 2018.
4. Montazeri K, Sonpavde G. Salvage systemic therapy for metastatic urothelial carcinoma: an unmet clinical need. *Expert Rev Anticancer Ther.* 2021;21(3):299-313.
5. Hurst CD, et al. Genomic Subtypes of Non-invasive Bladder Cancer with Distinct Metabolic Profile and Female Gender Bias in KDM6A Mutation Frequency. *Cancer cell.* 2017;32(5):701-715.e707.
6. Hodges C, et al. The Many Roles of BAF (mSWI/SNF) and PBAF Complexes in Cancer. *Cold Spring Harb Perspect Med.* 2016;6(8).
7. Mathur R. ARID1A loss in cancer: Towards a mechanistic understanding. *Pharmacol Ther.* 2018;190:15-23.
8. Wiegand KC, et al. ARID1A mutations in endometriosis-associated ovarian carcinomas. *N Engl J Med.* 2010;363(16):1532-1543.
9. Gao X, et al. ES cell pluripotency and germ-layer formation require the SWI/SNF chromatin remodeling component BAF250a. *Proc Natl Acad Sci U S A.* 2008;105(18):6656-6661.
10. Varambally S, et al. The polycomb group protein EZH2 is involved in progression of prostate cancer. *Nature.* 2002;419(6907):624-629.
11. Kleer CG, et al. EZH2 is a marker of aggressive breast cancer and promotes neoplastic transformation of breast epithelial cells. *Proc Natl Acad Sci U S A.* 2003;100(20):11606-11611.
12. Bracken AP, et al. EZH2 is downstream of the pRB-E2F pathway, essential for proliferation and amplified in cancer. *EMBO J.* 2003;22(20):5323-5335.
13. Kim KH, Roberts CW. Targeting EZH2 in cancer. *Nat Med.* 2016;22(2):128-134.
14. Margueron R, Reinberg D. The Polycomb complex PRC2 and its mark in life. *Nature.* 2011;469(7330):343-349.
15. Cao Q, et al. Repression of E-cadherin by the polycomb group protein EZH2 in cancer. *Oncogene.* 2008;27(58):7274-7284.
16. Yu J, et al. A polycomb repression signature in metastatic prostate cancer predicts cancer outcome. *Cancer Res.* 2007;67(22):10657-10663.
17. Weikert S, et al. Expression levels of the EZH2 polycomb transcriptional repressor correlate with aggressiveness and invasive potential of bladder carcinomas. *Int J Mol Med.* 2005;16(2):349-353.
18. Zhang YB, et al. EZH2 silencing by RNA interference inhibits proliferation in bladder cancer cell lines. *Eur J Cancer Care (Engl).* 2011;20(1):106-112.
19. Morschhauser F, et al. Tazemetostat for patients with relapsed or refractory follicular lymphoma: an open-label, single-arm, multicentre, phase 2 trial. *Lancet Oncol.* 2020;21(11):1433-1442.
20. Eich ML, et al. EZH2-targeted therapies in cancer: hype or a reality. *Cancer Res.* 2020.
21. Gounder M, et al. Tazemetostat in advanced epithelioid sarcoma with loss of INI1/SMARCB1: an international, open-label, phase 2 basket study. *Lancet Oncol.* 2020;21(11):1423-1432.
22. Bitler BG, et al. Synthetic lethality by targeting EZH2 methyltransferase activity in ARID1A-mutated cancers. *Nat Med.* 2015;21(3):231-238.
23. Kim KH, et al. SWI/SNF-mutant cancers depend on catalytic and non-catalytic activity of EZH2. *Nat Med.* 2015;21(12):1491-1496.
24. Wu S, et al. SWI/SNF catalytic subunits' switch drives resistance to EZH2 inhibitors in ARID1A-mutated cells. *Nat Commun.* 2018;9(1):4116.

25. Fukumoto T, et al. Repurposing Pan-HDAC Inhibitors for ARID1A-Mutated Ovarian Cancer. *Cell Rep.* 2018;22(13):3393-3400.
26. Balla T. Phosphoinositides: tiny lipids with giant impact on cell regulation. *Physiol Rev.* 2013;93(3):1019-1137.
27. Brachmann SM, et al. Role of phosphoinositide 3-kinase regulatory isoforms in development and actin rearrangement. *Mol Cell Biol.* 2005;25(7):2593-2606.
28. Burke JE. Structural Basis for Regulation of Phosphoinositide Kinases and Their Involvement in Human Disease. *Mol Cell.* 2018;71(5):653-673.
29. Ito Y, et al. Isoform-specific activities of the regulatory subunits of phosphatidylinositol 3-kinases - potentially novel therapeutic targets. *Expert Opin Ther Targets.* 2018;22(10):869-877.
30. Raghu P, et al. Phosphoinositides: Regulators of Nervous System Function in Health and Disease. *Front Mol Neurosci.* 2019;12:208.
31. Zhu S, et al. Synergistic antitumor activity of pan-PI3K inhibition and immune checkpoint blockade in bladder cancer. *Journal of ImmunoTherapy of Cancer.* 2021.
32. Pan CX, et al. Development and Characterization of Bladder Cancer Patient-Derived Xenografts for Molecularly Guided Targeted Therapy. *PLoS One.* 2015;10(8):e0134346.
33. Zeng SX, et al. The Phosphatidylinositol 3-Kinase Pathway as a Potential Therapeutic Target in Bladder Cancer. *Clin Cancer Res.* 2017;23(21):6580-6591.
34. Fruman DA, et al. The PI3K Pathway in Human Disease. *Cell.* 2017;170(4):605-635.
35. Vanhaesebroeck B, et al. The emerging mechanisms of isoform-specific PI3K signalling. *Nat Rev Mol Cell Biol.* 2010;11(5):329-341.
36. Goncalves MD, et al. Phosphatidylinositol 3-Kinase, Growth Disorders, and Cancer. *N Engl J Med.* 2018;379(21):2052-2062.
37. Zhu Z, et al. PI3K is negatively regulated by PIK3IP1, a novel p110 interacting protein. *Biochem Biophys Res Commun.* 2007;358(1):66-72.
38. von der Maase H, et al. Long-term survival results of a randomized trial comparing gemcitabine plus cisplatin, with methotrexate, vinblastine, doxorubicin, plus cisplatin in patients with bladder cancer. *J Clin Oncol.* 2005;23(21):4602-4608.
39. Sonpavde G. PD-1 and PD-L1 Inhibitors as Salvage Therapy for Urothelial Carcinoma. *N Engl J Med.* 2017;376(11):1073-1074.
40. Rosenberg JE, et al. Pivotal Trial of Enfortumab Vedotin in Urothelial Carcinoma After Platinum and Anti-Programmed Death 1/Programmed Death Ligand 1 Therapy. *J Clin Oncol.* 2019;37(29):2592-2600.
41. Garczyk S, et al. ARID1A-deficiency in urothelial bladder cancer: No predictive biomarker for EZH2-inhibitor treatment response? *PLoS One.* 2018;13(8):e0202965.
42. Hoy SM. Tazemetostat: First Approval. *Drugs.* 2020;80(5):513-521.
43. Yang Y, et al. Microarray pathway analysis indicated that mitogen-activated protein kinase/extracellular signal-regulated kinase and insulin growth factor 1 signaling pathways were inhibited by small interfering RNA against AT-rich interactive domain 1A in endometrial cancer. *Oncol Lett.* 2018;15(2):1829-1838.
44. He X, et al. PIK3IP1, a negative regulator of PI3K, suppresses the development of hepatocellular carcinoma. *Cancer Res.* 2008;68(14):5591-5598.
45. Chou TC. Drug combination studies and their synergy quantification using the Chou-Talalay method. *Cancer Res.* 2010;70(2):440-446.
46. Chandrashekar DS, et al. Therapeutically actionable PAK4 is amplified, overexpressed, and involved in bladder cancer progression. *Oncogene.* 2020;39(20):4077-4091.
47. Chakravarthi B, et al. A Role for De Novo Purine Metabolic Enzyme PAICS in Bladder Cancer Progression. *Neoplasia.* 2018;20(9):894-904.

48. Hossain MI, et al. Restoration of CTSD (cathepsin D) and lysosomal function in stroke is neuroprotective. *Autophagy.* 2021;17(6):1330-1348.

FIGURES AND LEGENDS:

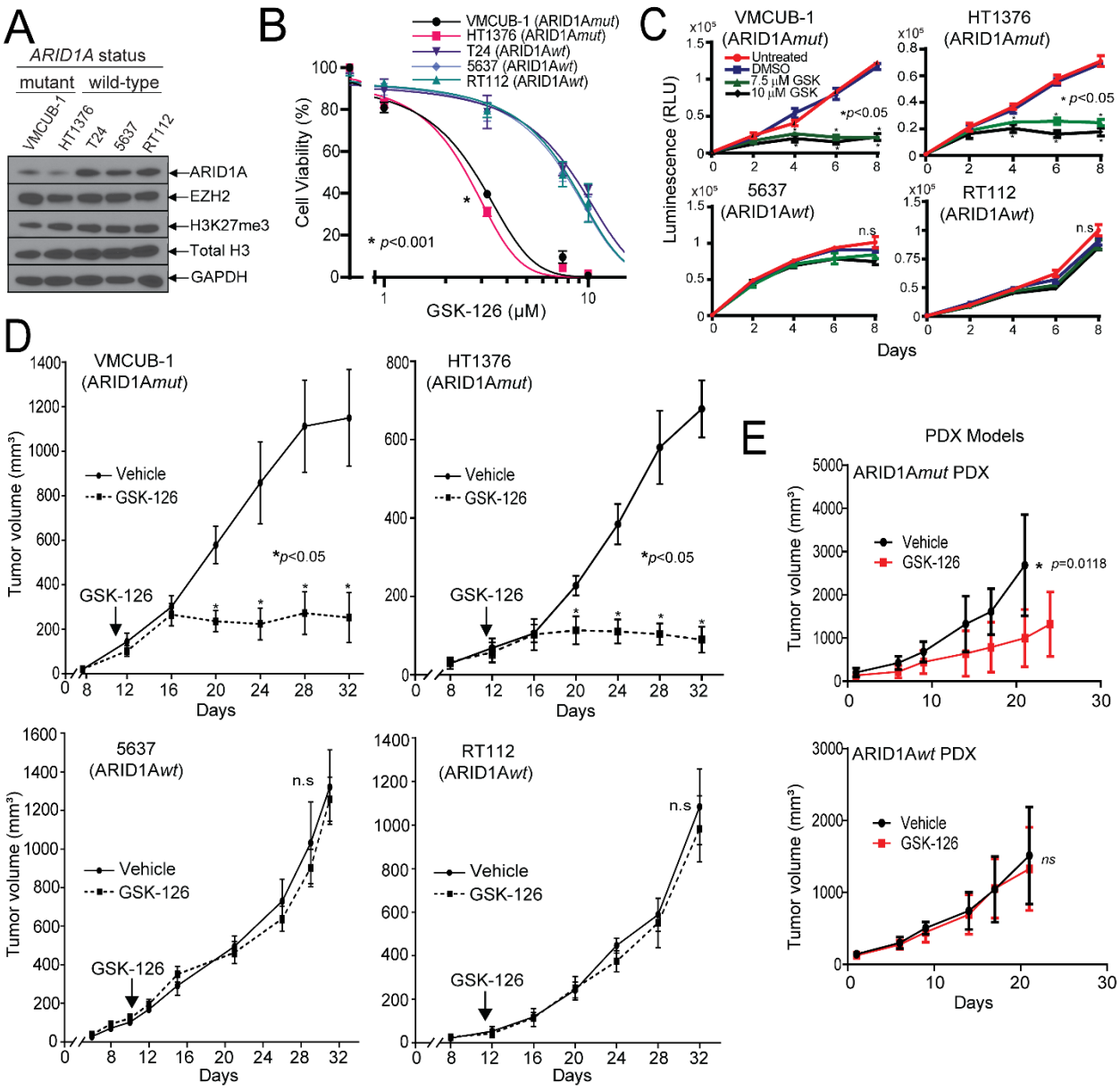

Figure 1: **Bladder cancer cells and xenografts with inactivating ARID1A mutations are sensitive to EZH2 inhibition.** (A) Immunoblots showing lower protein levels of ARID1A in bladder cancer cell lines harboring heterozygous *ARID1A*-truncating mutations (HT1376 and VMCUB-1), compared with ARID1A*wt* alleles (T24, 5637, and RT112). (B) Cell viability dose-response assay showing that ARID1A*mut* bladder cancer cells are more sensitive to the EZH2 inhibitor, GSK-126 (treated for 6d). Two-way ANOVA using IC-50 values was performed. (C) Cell viability time course with increasing concentrations of GSK-126 indicating that ARID1A*mut* cell lines are more sensitive than ARID1A*wt* cell lines. (D) Xenografts from ARID1A*mut* cells are sensitive to GSK-126, whereas ARID1A*wt* xenografts are resistant. (E) Xenografts (PDX) derived from bladder cancers with *ARID1A* mutations are more sensitive to GSK-126 than ARID1A*wt* xenografts. T-tests were performed, unless otherwise specified. N.S. denotes "non-specific".

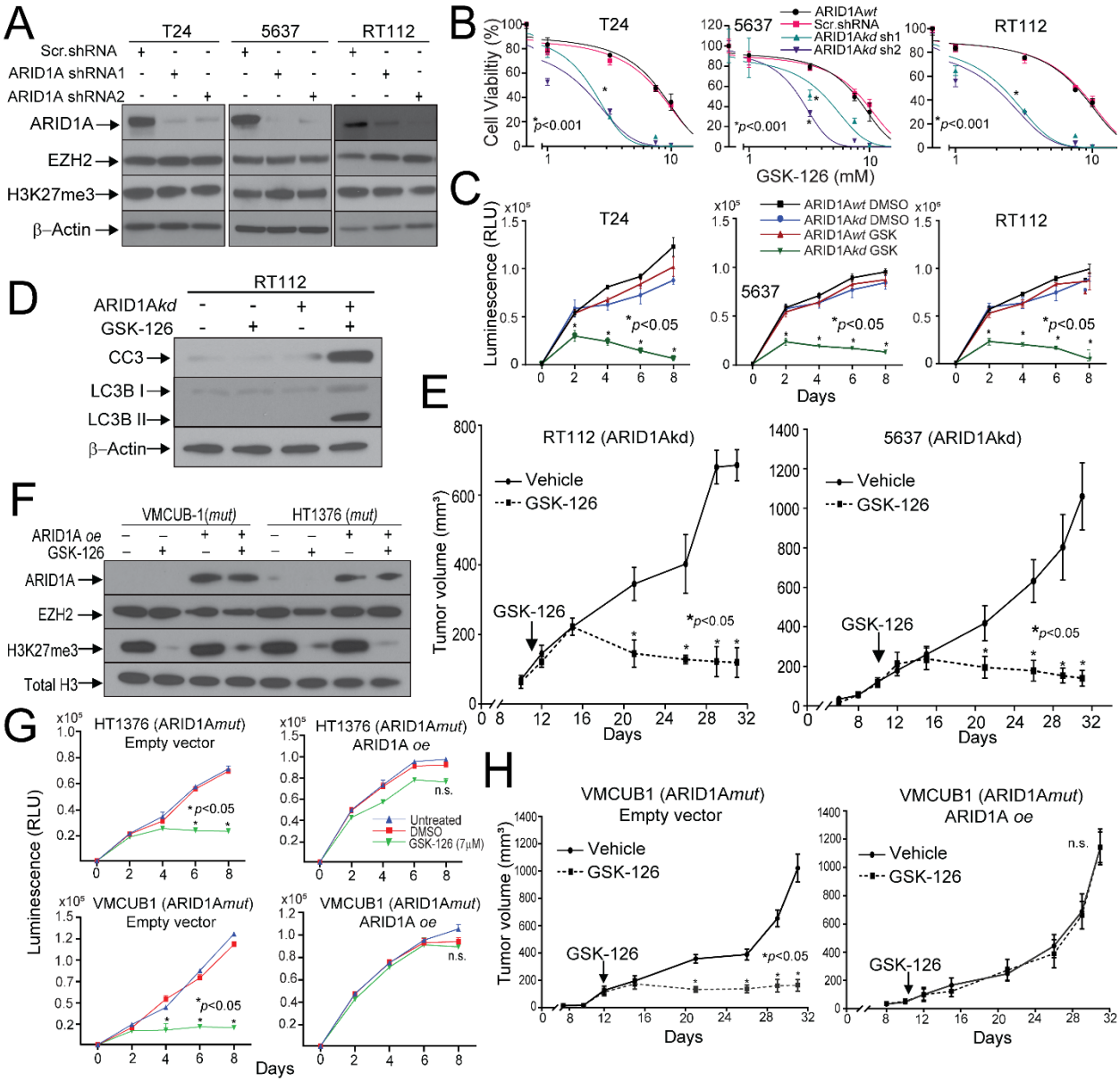

Figure 2: **ARID1A deficiency in bladder cancer cells is necessary and sufficient for sensitivity to EZH2 inhibition.** (A) Immunoblots showing expression of ARID1A, EZH2, and tri-methylated H3K27 (H3K27me3) in ARID1A*wt* bladder cancer cell lines after ARID1A stable knockdown (KD) with two separate shRNA sequences along with scrambled (scr) shRNA. (B) Cell viability dose-response assay showing that ARID1A*kd* bladder cancer cells are more sensitive to the EZH2 inhibitor GSK126 than scr shRNA controls (treatment for 6 d). Two-way ANOVA using IC-50 values was performed. (C) Cell viability time course with GSK-126 treatment showing that ARID1A*kd* cells are more sensitive than ARID1A*wt* cells. (D) Immunoblot for cleaved caspase 3 (CC3) and LC3BII indicating that apoptosis and autophagy are activated in ARID1A*kd* cells treated with GSK-126 for 48 h. (E) Xenografts from mice inoculated with ARID1A*kd* cells showing that these tumors are sensitive to GSK-126 treatment. (F) Immunoblot analysis of ARID1A*mut* cell lines stably transduced with ARID1A overexpression (oe) lentivirus or empty vector control and treated with GSK-126 for 48 h. (G) Cell proliferation assays using ARID1A*mut* cell lines with or without ARID1A*oe* indicating that sensitivity to GSK-126 is abrogated by ARID1A reconstitution. (H) Xenografts from ARID1A*mut* cell lines with ARID1A*oe* are resistant to GSK-126 inhibition. T-tests were performed unless otherwise specified. N.S. denotes "non-specific".

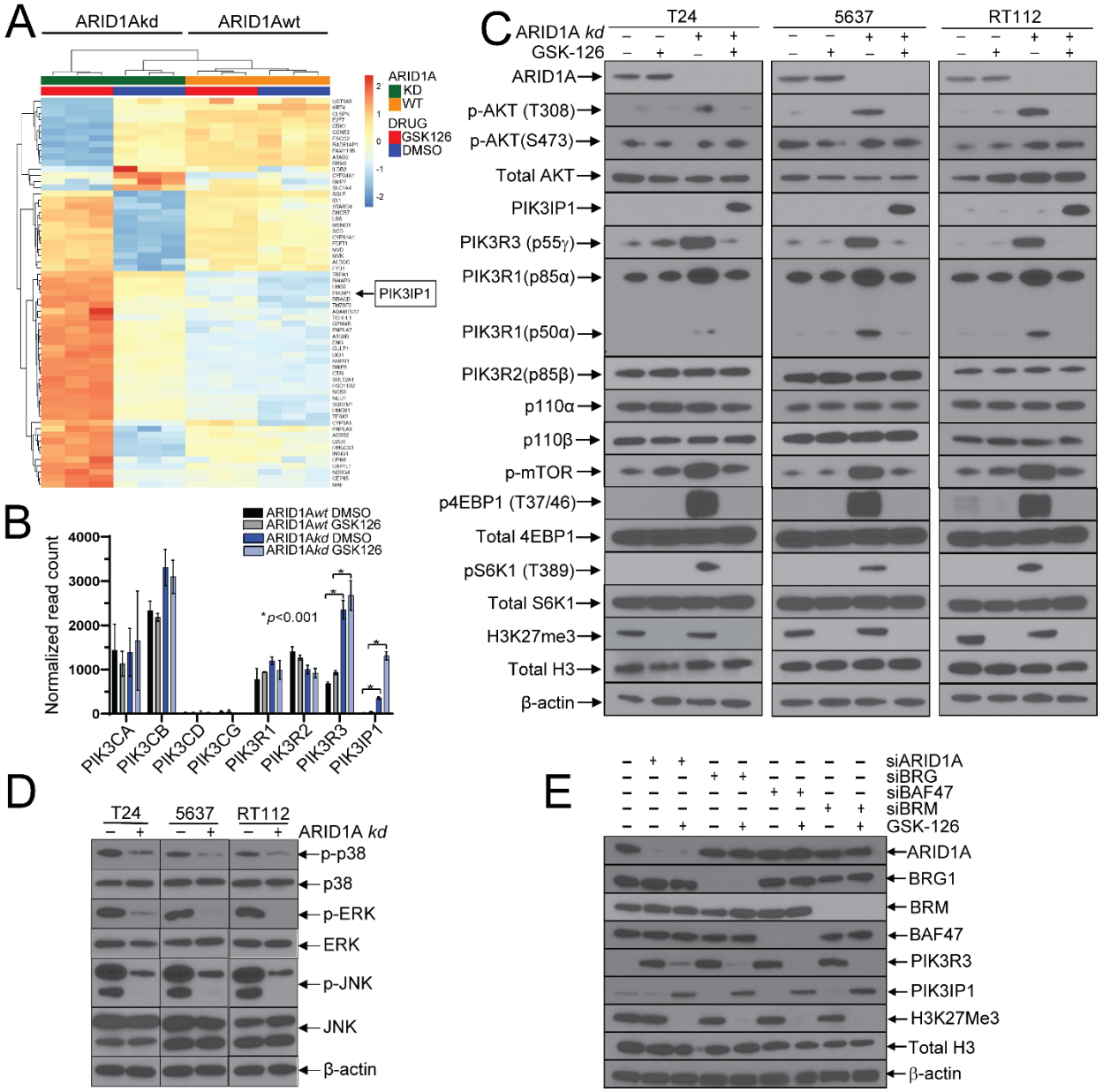

Figure 3: **ARID1A deficiency leads to upregulation of PI3K signaling and downregulation of MAPK signaling, which results in a dependency on PI3K signaling. This dependency is targeted by GSK-126-mediated upregulation of the endogenous PI3K inhibitor, PIK3IP1.** (A) Dendogram from whole transcriptomic RNAseq analysis showing differentially expressed genes between RT112 ARID1A*wt* cells treated with GSK-126 (5 μM for 24 h) and RT112 ARID1A*kd* cells treated with GSK-126. PIK3IP1 is a putative tumor suppressor, an inhibitor of PI3K signaling, and a candidate for GSK-126 sensitivity in ARID1A*def* cells. (B) RNAseq subgroup analysis of major PI3K catalytic and regulatory subunits showing that PIK3R3 is upregulated in ARID1A*kd* cells. T-tests were performed. (C) Immunoblot of major PI3K/AKT/mTOR signaling cascade constituents showing that PIK3R3/p55γ (and to a lesser extent PIK3R1/p85α/p50α) are upregulated in ARID1A*kd* cells and correspond with activation of AKT and downstream mTOR targets, p4EBP1 and pS6K1. These changes are abrogated upon treatment with GSK-126 (5 μM for 48 h), which correlates with upregulation of PIK3IP1. (D) Immunoblots of ARID1A*kd* and ARID1A*wt* cells revealing downregulation of MAPK signaling in ARID1A*kd* cells, including p38, ERK, and JNK. (E) Immunoblot of RT112 cells with siRNA mediated knockdown of various SWI/SNF (BAF) components as indicated with and without GSK-126 treatment shows that an intact complex is necessary to inhibit PIK3R3 expression and prevent GSK-126 mediated upregulation of PIK3IP1.

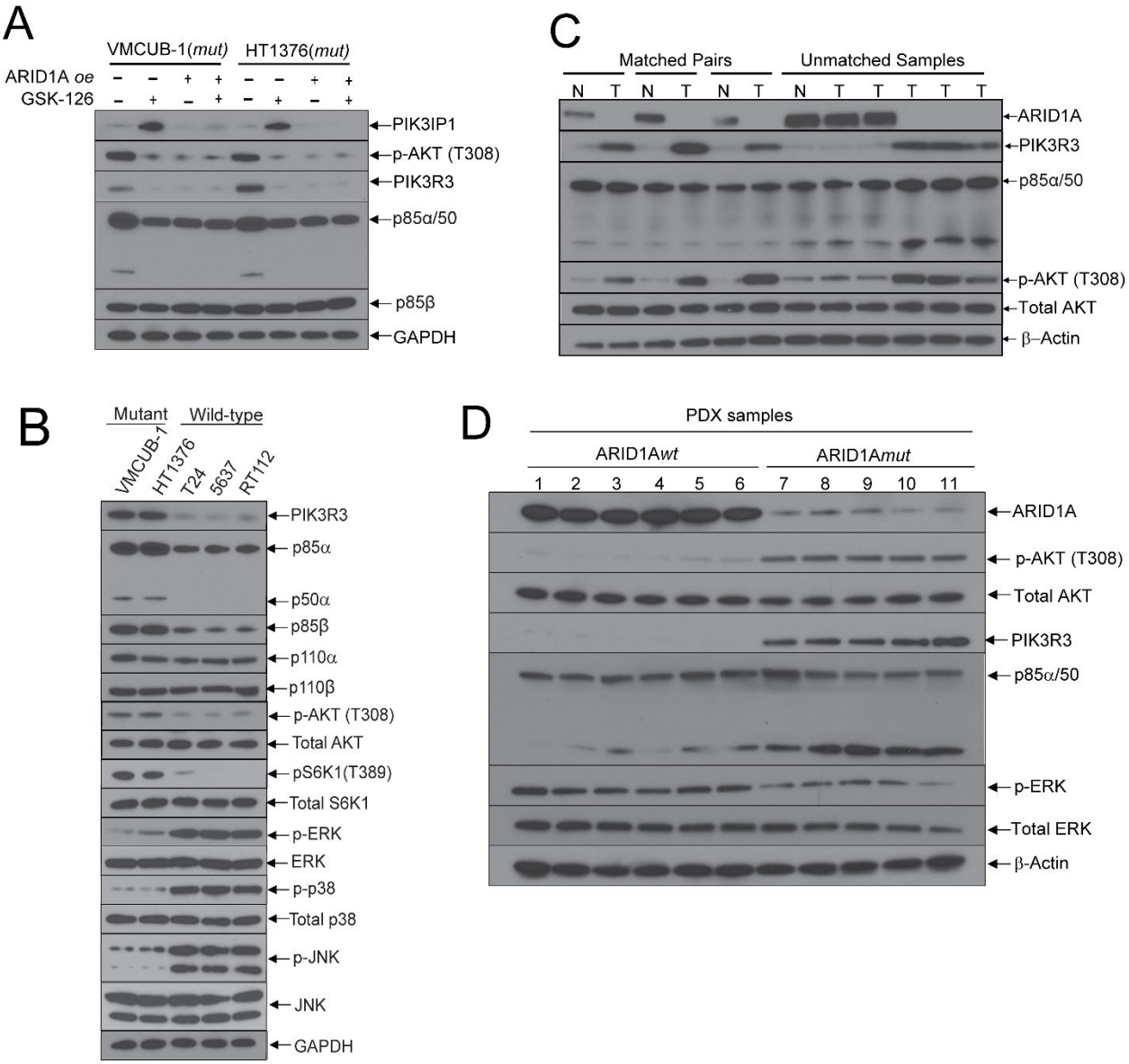

Figure 4: **ARID1A deficiency correlates with upregulation of PIK3R3, activation of the PI3K/AKT signaling cascade, and downregulation of MAPK signaling in human bladder cancers.** (A) Immunoblot of ARID1A overexpressing (*oe)* cells with or without GSK-126 (5 μM for 48 h), showing that PIK3IP1 upregulation with GSK-126 treatment is abrogated by ARID1A reconstitution. These blots are from the same experiment shown in Figure 2F. (B) Immunoblots of bladder cancer cells with or without ARID1A mutations indicating that ARID1A deficiency correlates with PI3K upregulation and MAPK downregulation. (C) Immunoblots of lysates from bladder tumors (T) and matched adjacent normal tissue (N) (as well as unmatched samples), from patients undergoing cystectomy showing that tissues deficient in ARID1A have high levels of PIK3R3 and activated AKT. (D) Immunoblots using lysates from PDX models with ARID1A*wt* and *mut* alleles indicates that ARID1A deficiency correlates with increased PIK3R3 and pAKT, and decreased MAPK activation. Corresponding sample numbers are noted in methods.

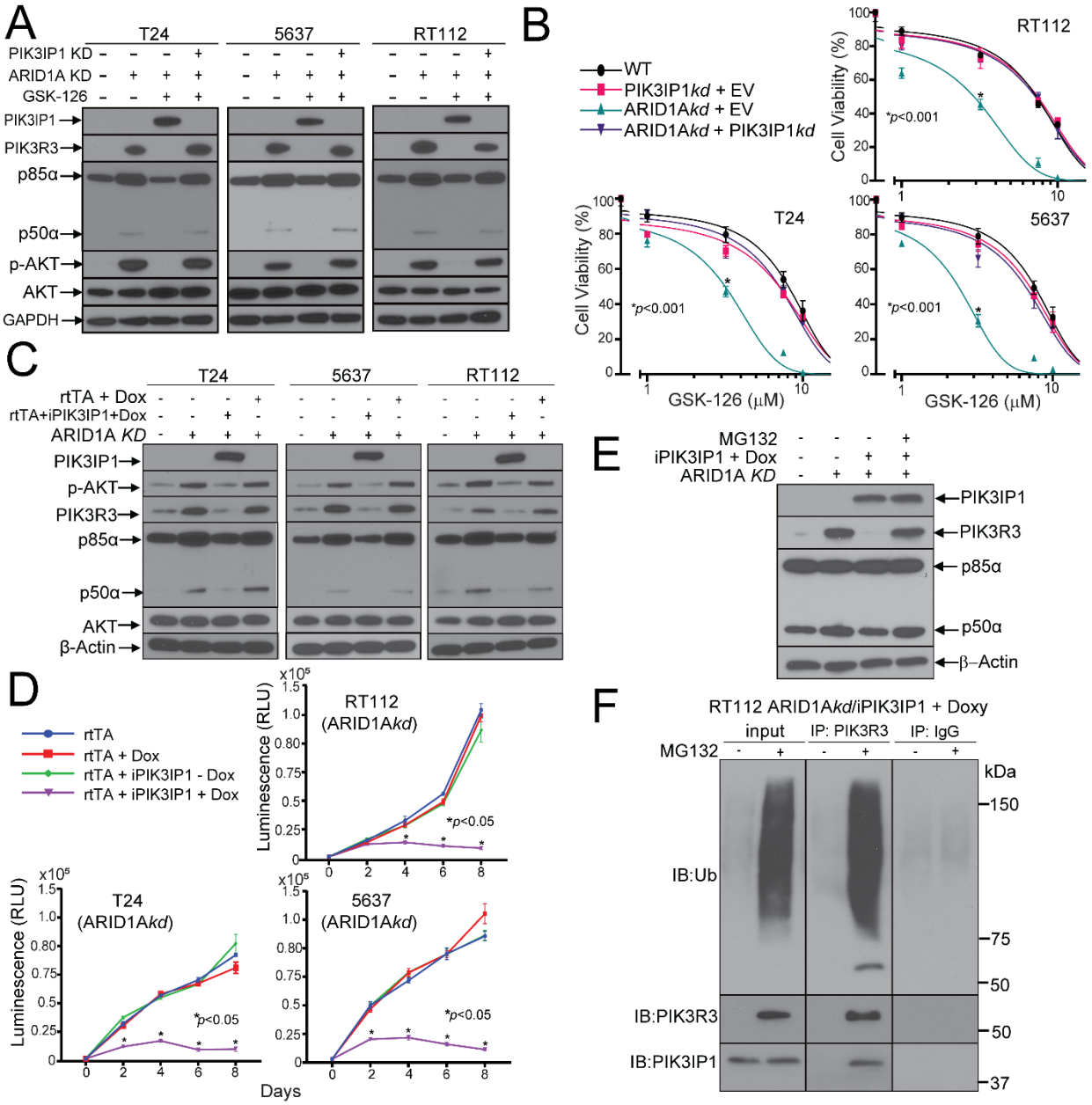

Figure 5: **PIK3IP1 is necessary and sufficient for decreased viability of ARID1A*kd* cells, and functions by inducing proteasomal degradation of PIK3R3.** (A) Immunoblot analysis of PI3K constituents in ARID1A*kd*/PIK3IP1*kd* cells vs ARID1A*kd*/empty vector cells showing that PIK3IP1 upregulation upon GSK-126 treatment (5 μM for 48 h) is necessary to downregulate PIK3R3 and AKT activation. (B) Cell viability dose-response analysis with GSK-126 6-day treatment of ARID1A*kd*/PIK3IP1*kd* cells or empty vector (EV) controls showing that PIK3IP1*kd* is sufficient to rescue the GSK-126 sensitivity phenotype in ARID1A*kd* cells. T-test using IC-50 values was performed. (C) Immunoblot analysis of ARID1A*kd* cell lines stably transfected with doxycycline-inducible PIK3IP1 (iPIK3IP1) showing that PIK3IP1 overexpression results in downregulation of PIK3R3 and AKT activation. rtTA denotes vector encoding doxycycline-inducible transcriptional modulators (without inducible PIK3IP1). (D) Cell proliferation time course using the ARID1A*kd* cell lines in (C) showing that PIK3IP1 overexpression results in less proliferation. T-tests were performed. (E) Co-treatment of ARID1A*kd*/PIK3IP1-doxycycline-inducible cells with doxycycline and the proteasome inhibitor MG132 (15 μM for 12 h) prevented PIK3R3 downregulation upon PIK3IP1 overexpression. (F) Co-treatment of ARID1Akd/iPIK3IP1 cells with doxycycline and MG-132, followed by immunoprecipitation of PIK3R3 resulted in co-immunoprecipitation of PIK3IP1 and poly-ubiquitination signal.

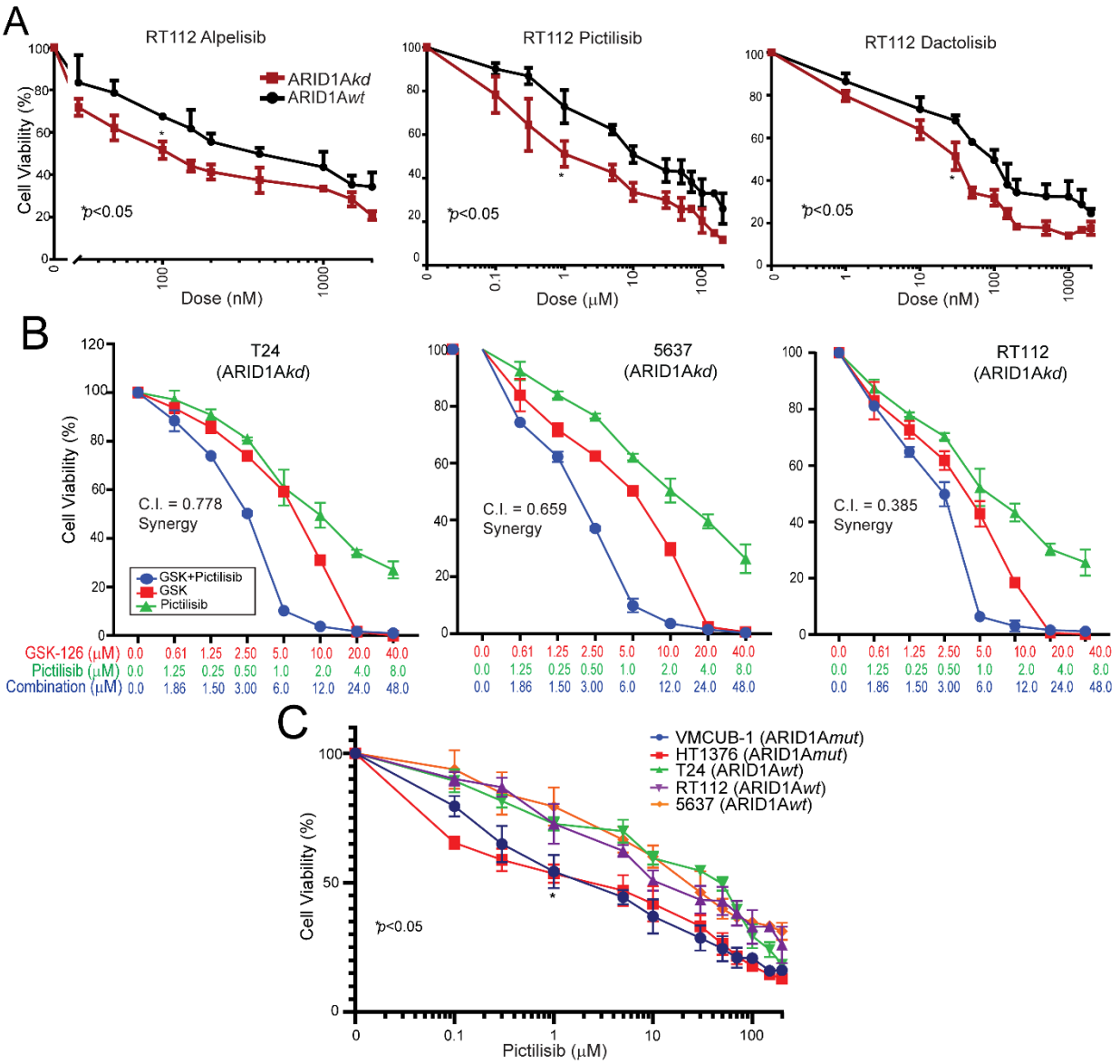

Figure 6: **ARID1A deficiency sensitizes bladder cancer cells to PI3K inhibitors, which act synergistically with GSK-126.** (A) Cell viability dose-response analysis of RT112 cells with ARID1A*kd* or empty vector (ARID1A*wt*) treated with alpelisib (a PI3K alpha-selective inhibitor), pictilisib (a PI3K class I selective inhibitor), or dactolisib (a dual PI3K/mTOR inhibitor) (all 48 h). T-tests of IC50 values were performed. (B) Dose-response synergy analyses were performed with GSK-126 and pictilisib using ARID1A*kd* cell lines (48 h). Combination indices (CI) and synergism were calculated using the Chou-Talalay method. (C) Dose-response cell viability curves of bladder cancer cells with ARID1A wild-type and mutant alleles (48 h treatment). Two-way ANOVA was performed using IC-50 values.

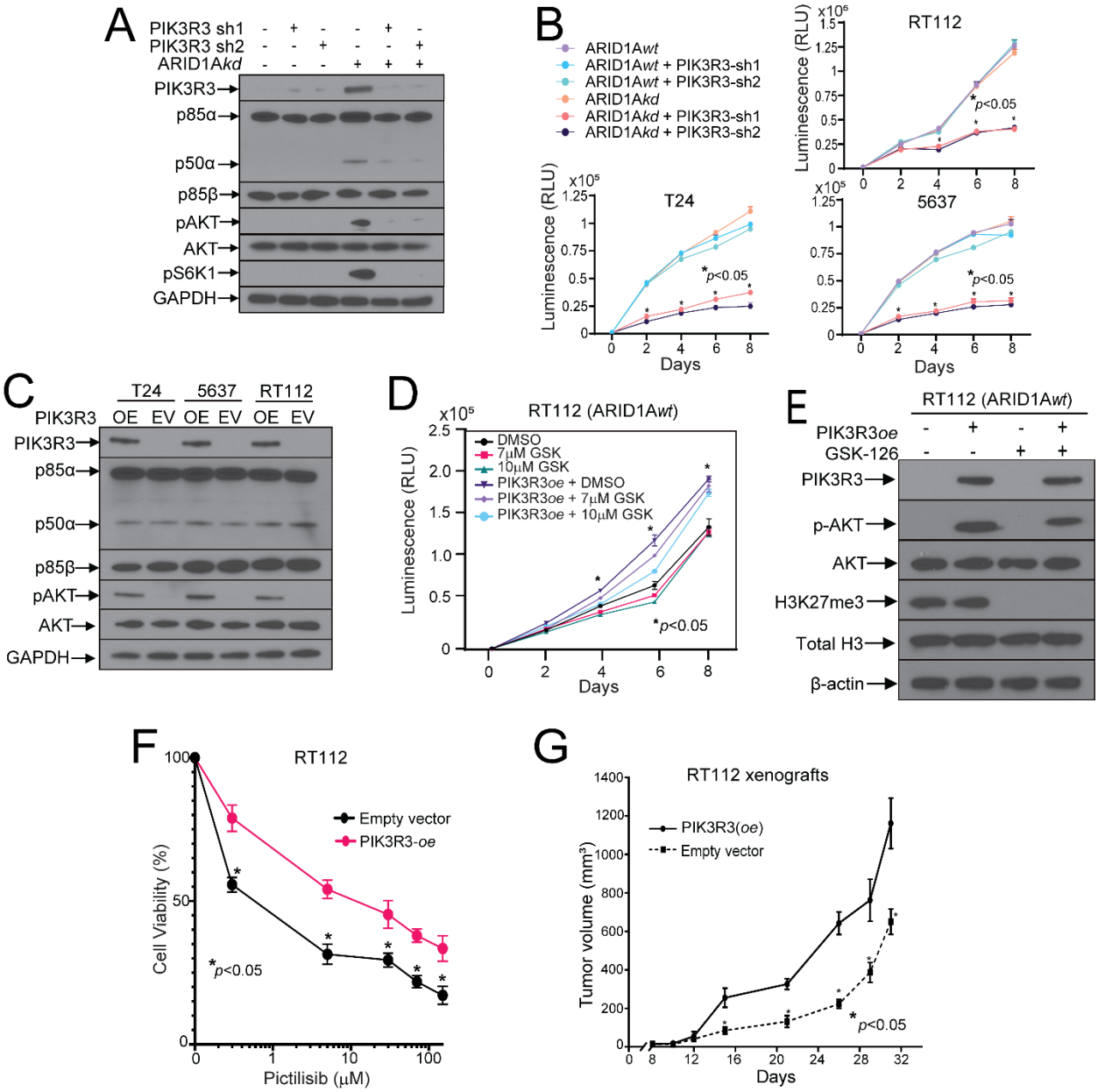

Figure 7: **PIK3R3 upregulation in ARID1A*kd* cells is necessary and sufficient for bladder cancer cell proliferation, but is not sufficient to convey GSK-126 or PI3K inhibitor sensitivity.** (A) Immunoblots of lysates of RT112 ARID1A*kd* cells with PIK3R3 shRNA constructs (or empty vector) indicating that PIK3R3 KD prevents AKT and mTOR activation. (B) PIK3R3 KD inhibited proliferation of ARID1A*kd* cells, but not ARID1A*wt* cells. T-tests were performed. (C) PIK3R3 overexpression (OE) in ARID1A*wt* cells increased AKT activation compared with cells transfected with an empty vector (EV). (D) RT112 cells with PIK3R3 overexpression show increased proliferation at baseline, but no increased sensitivity to GSK-126. Two-way ANOVA was performed. (E) Lysates from (D) indicating that GSK-126 (5 μM for 48 h) inhibits H3K27 trimethylation in these cells. (F) Dose-response assay using RT112 ARID1A*wt* cells with PIK3R3 overexpression or empty vector showing that PIK3R3 overexpression causes resistance to the PI3K inhibitor, pictilisib (48 h). T-tests were performed. (G) Xenografts of RT112 ARID1A*wt* cells with PIK3R3 overexpression grow faster than cells transfected with empty vector controls. T-tests were performed.

Potential Conflicts of Interest:

G.S.: **Advisory Board:** BMS, Genentech, EMD Serono, Merck, Sanofi, Seattle Genetics/Astellas, Astrazeneca, Exelixis, Janssen, Bicycle Therapeutics, Pfizer, Immunomedics/Gilead, Scholar Rock, G1 Therapeutics, Eli Lilly/Loxo Oncology, Infinity Pharmaceuticals, Lucence health, IMV; **Research Support to Institution:** Sanofi, Astrazeneca, Immunomedics/Gilead, QED, Predicine, BMS, EMD Serono, Jazz Therapeutics; **Steering committee of studies**: BMS, Bavarian Nordic, Seattle Genetics, QED, G1 Therapeutics (all unpaid), and Astrazeneca, EMD Serono, Debiopharm (paid); **Data safety monitoring committee**: Mereo; **Travel costs**: BMS, Astrazeneca; **Employment**: spouse employed by Myriad Genetics; Writing/**Editor fees**: Uptodate, Editor of Elsevier Practice Update Bladder Cancer Center of Excellence; **Speaking fees**: Physicians Education Resource, Onclive, Research to Practice, Medscape, Cancer Network, Masters Lecture Series (MLS).